



Title	Band structures of passive films on titanium in simulated bioliquids determined by photoelectrochemical response: principle governing the biocompatibility
Author(s)	Kim, Seong Cheol; Hanawa, Takao; Manaka, Tomoyo et al.
Citation	Science and Technology of Advanced Materials. 2022, 23(1), p. 322-331
Version Type	VoR
URL	<a href="https://hdl.handle.net/11094/88666">https://hdl.handle.net/11094/88666</a>
rights	
Note	

*The University of Osaka Institutional Knowledge Archive : OUKA*

<https://ir.library.osaka-u.ac.jp/>

The University of Osaka

# Band structures of passive films on titanium in simulated bioliquids determined by photoelectrochemical response: principle governing the biocompatibility

Seong-Cheol Kim <sup>a</sup>, Takao Hanawa <sup>a,b,c</sup>, Tomoyo Manaka <sup>d</sup>, Hiroaki Tsuchiya <sup>a</sup> and Shinji Fujimoto <sup>a</sup>

<sup>a</sup>Division of Materials and Manufacturing Science, Graduate School of Engineering, Osaka University, Suita, Osaka, Japan;

<sup>b</sup>Institute of Biomaterials and Bioengineering, Tokyo Medical and Dental University (TMDU), Tokyo, Japan;

<sup>c</sup>Center for Advanced Medical Engineering Research and Development, Kobe University, Kobe, Japan;

<sup>d</sup>Graduate school of Medical and Dental Sciences, Tokyo Medical and Dental University (TMDU), Tokyo, Japan

## ABSTRACT

The band structures and band gap energies,  $E_g$ , of passive films formed on titanium (Ti) in simulated bioliquids, Hanks' solution (Hanks) and saline, were evaluated. Ti was polarized at 0, −0.1, and −0.2 V<sub>Ag/AgCl</sub>,  $E_{tr}$  for 1 h. After polarization, the surfaces were characterized using X-ray photoelectron spectroscopy, and the photoelectrochemical responses were evaluated. The current change during photoirradiation was recorded as a photocurrent transient at each measuring potential,  $E_m$ , and by changing the wavelength of the incident light. Passive films consisted of a very thin TiO<sub>2</sub> layer containing small amounts of Ti<sub>2</sub>O<sub>3</sub> and TiO, hydroxyl groups, and water. During polarization in Hanks, calcium and phosphate ions were incorporated or formed calcium phosphate but not in saline. Calcium phosphate and hydroxyl groups influenced the band structure.  $E_g$  was graded in Hanks but constant in saline, independent of  $E_f$  and  $E_m$ . The passive film on Ti behaved as an *n*-type semiconductor containing two layers: an inner oxide layer with a large  $E_g$  and an outer hydroxide layer with a small  $E_g$ . In Hanks,  $E_g$  was 3.3–3.4 eV in the inner oxide layer and 2.9 eV in the outer hydroxide layer. In saline,  $E_g$  was 3.3 eV in the inner layer and 2.7 eV in the outer layer. Calcium phosphate and hydroxyl groups influenced the band structure of the passive film. The  $E_g$  of the outermost surface was smaller than that of TiO<sub>2</sub> ceramics, which is probably one of the principles of the excellent biocompatibility of Ti among metals.

## ARTICLE HISTORY

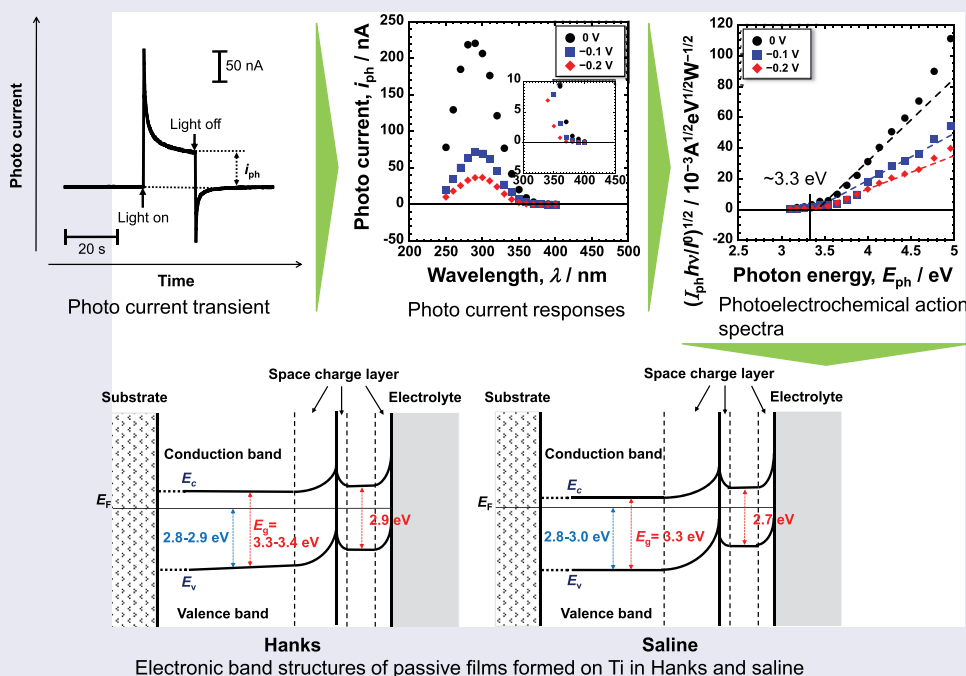
Received 12 February 2022



Revised 1 April 2022


Accepted 11 April 2022

## KEYWORDS

band gap; band structure; biocompatibility; Hanks' solution; passive film; photocurrent; saline; Titanium; XPS



**CONTACT** Takao Hanawa  [hanawa.met@tmd.ac.jp](mailto:hanawa.met@tmd.ac.jp)  Institute of Biomaterials and Bioengineering, Tokyo Medical and Dental University, 2-3-10 Kanda-surugadai, Chiyoda-ku, Tokyo 101-0062, Japan

 Supplemental data for this article can be accessed online at <https://doi.org/10.1080/14686996.2022.2066960>.

© 2022 The Author(s). Published by National Institute for Materials Science in partnership with Taylor & Francis Group.

This is an Open Access article distributed under the terms of the Creative Commons Attribution License (<http://creativecommons.org/licenses/by/4.0/>), which permits unrestricted use, distribution, and reproduction in any medium, provided the original work is properly cited.

## 1. Introduction

Titanium (Ti) and its alloys are widely used as implant devices in medicine and dentistry because of their excellent corrosion resistance and high specific strength [1]. Their good tissue compatibility is well established through significant evidence from basic research and high clinical performance. For example, in orthopedics, bone screws and bone nails consisting of Ti alloys usually form calluses and assimilate into bone tissue after long-term implantation, inducing refracture of the bone during retrieval [2]. This is because of the good compatibility of Ti alloys with hard tissues. Many studies on the hard-tissue compatibility of Ti have been performed, and detailed information can be found in the literature [1,3]. The initial reaction at the interface directly influences the biocompatibility of the material. Therefore, biocompatibility is governed by the surface properties of the material. However, the principle and mechanism of the good tissue compatibility of Ti among metals have not been completely elucidated, despite numerous studies conducted on biological reactions.

The Ti metal surface is covered by a passive oxide film, which contributes to its excellent corrosion resistance. The passive film on Ti is mainly an extremely thin amorphous  $\text{TiO}_2$  containing small amounts of  $\text{Ti}_2\text{O}_3$  and  $\text{TiO}$ , along with water and hydroxyl groups [4–7]. In addition, as the composition is graded, more  $\text{Ti}^{4+}$  and  $\text{OH}^-$  ions appear near the surface of the film [6]. This passive film formation process has been discussed elsewhere [8], and the chemical state of the passive oxide film has also been precisely investigated [9]. It has been established that the composition, structure, and chemical state of the passive film are different from those of the crystalline  $\text{TiO}_2$  ceramics. For example, the adsorption kinetics of calcium and phosphate ions in passive films on Ti differ from those in  $\text{TiO}_2$  ceramics [10].

In this regard, the band gap energy,  $E_g$ , between the valence and conduction bands of  $\text{TiO}_2$  crystalline ceramics is usually evaluated by the optical absorption edge. It is well known that the reactivity of  $\text{TiO}_2$  ceramics is governed by  $E_g$ , and continuous efforts to decrease  $E_g$  have been made to activate their photocatalytic performance [11]. The  $E_g$  of a photocatalyst decreases as its optical response shifts to longer excitation wavelengths. From this viewpoint, the passive film on Ti already contains oxygen defects because of its nonstoichiometric composition. Therefore, the difference in the surface properties of the passive films on Ti and  $\text{TiO}_2$  ceramics is probably due to the difference in their  $E_g$ s. The  $E_g$  of passive films on Ti after anodic oxidation and thermal oxidation has been investigated by the photoelectrochemical response in borate buffer solution, artificial seawater, and sulfuric acid [12–14]

because the conventional techniques employed for oxide ceramics, such as ultraviolet absorption, cannot be used for thin passive films on Ti.

In this study, the  $E_g$  values of passive films formed on Ti in simulated bioliquids, Hanks' solution and 0.9% NaCl aqueous solution, were evaluated using the photoelectrochemical response at potentials as close as possible to the open circuit potential (OCP). In addition, X-ray photoelectron spectroscopy (XPS) was performed to understand the effect of the chemical composition and chemical state of the passive films on the photoelectrochemical properties. This research will enhance our understanding of the properties of passive films on Ti in the human body.

## 2. Experimental procedure

### 2.1 Specimen

Commercially or industrially pure titanium (ISO grade 2; >99.5% Ti; Test Materials, Tokyo, Japan) rods (8 mm in diameter) were cut into disks (1.5 mm in thickness). In the case of OCP measurement and XPS, the disks were polished with SiC paper, followed by mirror finishing with a  $0.04\ \mu\text{m}$   $\text{SiO}_2$  suspension. After polishing, the Ti disks were ultrasonically cleaned twice in acetone and once in isopropanol for 10 min each. The Ti disks were immersed in ultrapure water for 24 h to stabilize the passive films. The disks were then fixed in a polytetrafluoroethylene holder with an o-ring, exposing an area of  $0.278\ \text{cm}^2$  to the electrolyte. For photoelectrochemical measurements, Ti was connected to a lead wire by soldering. The disks and connected parts were embedded in epoxy resin, and the surface was polished with SiC paper, followed by mirror finishing with a  $0.25\ \mu\text{m}$  diamond suspension. After polishing, the specimens were ultrasonically cleaned sequentially in acetone, ethanol, and deionized water for 10 min each and immediately used for subsequent experiments.

### 2.2 Electrolytes

Hanks' solution without glucose (Hanks) was prepared using reagent-grade chemicals in ultrapure water. The composition of the Hanks was similar to that of extracellular fluid which is as follows:  $\text{Na}^+$  142,  $\text{K}^+$  5.81,  $\text{Mg}^{2+}$  = 0.811,  $\text{Ca}^{2+}$  = 1.26,  $\text{Cl}^-$  = 145,  $\text{PO}_4^{3-}$  = 0.778,  $\text{SO}_4^{2-}$  = 0.811, and  $\text{CO}_3^{2-}$  = 4.17 (mmol/L). The pH of Hanks was 7.4 after preparation and did not change during the experimental acquisition at  $37^\circ\text{C}$ . A 0.9 mass% NaCl solution (saline) was also prepared for comparison. The pH of saline is 6.4 just after preparation at  $37^\circ\text{C}$ .

### 2.3 Open circuit potential change with time

The changes in OCP with time in Hanks and saline were measured using a Pt counter electrode and an Ag/AgCl reference electrode. The OCP was measured after 72 h of immersing the specimens in the electrolyte.

### 2.4 Photoelectrochemical response

The specimens were immersed in Hanks and saline for 10 min. The specimens were then polarized at film formation potentials,  $E_f$ , of  $-0.2$ ,  $-0.1$ , and  $0$  V versus Ag/AgCl electrode in Hanks and saline for 1 h to form stable passive films. These potentials were determined according to the change in the OCP for 72 h. The potentials were as close as possible to the OCP. The pH of the saline after polarization was 5.3–5.8.

The photoelectrochemical response of the passive films was investigated using an experimental equipment similar to that used in a previous study [15–18]. The photoelectrochemical responses were measured using a potentiostat connected to a low-pass filter with a threshold frequency of 4 Hz and a differential amplifier. Monochromatic light from a 150 W xenon arc lamp and a grating monochromator was irradiated onto Ti specimens in an electrochemical cell through a quartz window. Current changes during photoirradiation for 20 s were recorded as photocurrent transients at each  $E_f$ . The measurement was performed at each measuring potential,  $E_m$ , by decreasing  $E_f$  at regular intervals of 0.1 V with the wavelength of the incident light varying from 250 to 450 nm.

### 2.5 X-ray photoelectron spectroscopy

After polarization at each  $E_f$  in both Hanks and saline for 1 h, the Ti specimens were rinsed with ultrapure water to remove any chemical species not incorporated onto the surface and dried by a stream of  $N_2$  gas. Immediately after drying, the specimens were inserted in the pre-evacuation chamber of the XPS machine (JPS-9010MC, JEOL, Tokyo, Japan). Mg Ka line (1253.6 eV) was employed as the X-ray source. The binding energies were calibrated with the electron energy region of C 1s peak (285.0 eV) originating from the so-called contamination. The background of peaks was subtracted with Shirley's method [19]. The composition and thickness of the passive film were simultaneously calculated according to previous studies [20,21] that is outlined elsewhere [7,22,23]. The results were statistically evaluated using one-way ANOVA with a significance of  $p < .05$ .

## 3. Results

### 3.1 Change in open circuit potential

The pH of Hanks remained at 7.4 at 37°C, and no precipitation was observed during the OCP measurement; the pH of saline gradually decreased to 5.7 after 6 h and 5.8 after 72 h at 37°C. Changes in the OCP of Ti in Hanks and saline over time are shown in Figure 1. The OCP was between  $-0.2$  V and  $-0.3$  V in Hanks and saline just after starting the measurement and immediately decreased after immersion, followed by a gradual increase with time. After 72 h, the OCP was approximately  $-0.2$  V in Hanks and  $-0.1$  V in saline. The OCP in saline was always more noble than that in Hanks because the pH of saline was lower than that of Hanks.

### 3.2 Photoelectrochemical response

A typical photocurrent transient for passive films formed on Ti in Hanks and saline is shown in Figure 2. The shapes of the current transients in all the specimens were similar to that in this figure. The current varies during photoirradiation; therefore, the current recorded after 20 s was defined as the photocurrent,  $i_{ph}$ , for analysis in the present work.

Figure 3 shows the photocurrent responses of the passive films formed on Ti in Hanks and saline. The photocurrent varied depending on  $E_m$  and the wavelength of the incident light. The photocurrent spectra were normalized for further analysis because the intensity of the light is not constant for each wavelength. Assuming that the photoexcitation is generated as an indirect transition, the photocurrent spectra were normalized as a photoelectrochemical action spectrum as follows [15–18].

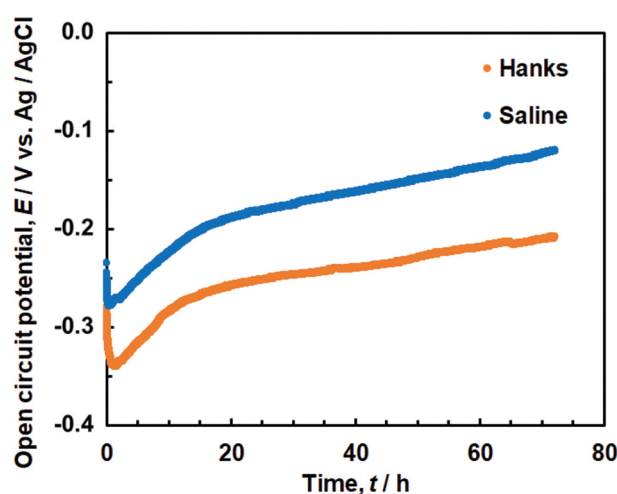
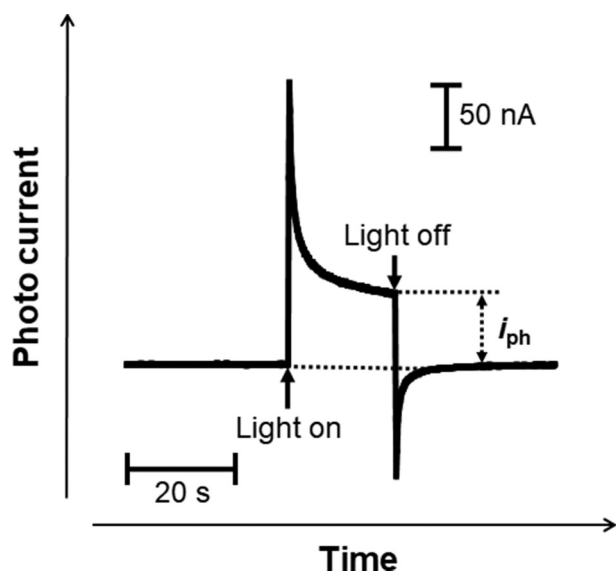


Figure 1. Change in open circuit potentials (OCP) of Ti in Hanks and saline for 72 h.



**Figure 2.** Example of photocurrent transient generated with the light on and off for passive films on Ti.

$$(i_{ph} \cdot h\nu / I_0)^{1/2} = C(h\nu - E_g), \quad (1)$$

where  $I_0$  and  $h\nu$  are the intensity and photon energy of the incident light, respectively,  $C$  is the slope of the photoelectrochemical action spectrum and reflects the amplitude of the generated photocurrent, and  $h$  is Planck's constant. By replotting the photocurrent spectra in [Figure 3](#), photoelectrochemical action spectra against the photon energy of irradiated light,  $E_{ph}$ , were obtained, as shown in [Figures 4 and 5](#), corresponding to the Hanks and

saline, respectively. The bottom figures show enlarged views of the lower photon energy region. In the case of Hanks, the photoelectrochemical action spectra did not exhibit a straight line with a constant  $C$ , instead  $C$  gradually changed. When the photocurrent is generated from a uniform composition layer, the direction of the photocurrent does not change at a fixed potential, even if the photon energy of the incident light is changed. In other words,  $E_g$  of the passive film was not uniform in the Hanks.

On subtracting the photoelectrochemical response of a component with lower band gap energy from the original photoelectrochemical action spectra, the photoelectrochemical action spectra for the other component with higher band gap energy are obtained in the higher photon energy region. The extrapolation of the remaining spectra on the horizontal axis represents a larger  $E_g$  component. The intersection between the extrapolation of the mean gradient lines and the horizontal axis represents  $E_g$ . For Hanks, the larger component of  $E_g$  was in the range of 3.3–3.4 eV.  $C$  decreased near the lower photoelectrochemical action region, and the intersection shows that the  $E_g$  was 2.9 eV. This value was identical for all the examined specimens in Hanks. In addition, the value of  $C$  for the  $E_f$  of  $-0.2$  V was negative. In the case of saline, the  $E_g$  was determined to be 3.3 eV. Near the lower photoelectrochemical action region,  $E_g$  was 2.7 eV. The band gap values in Hanks were larger than those in the saline.

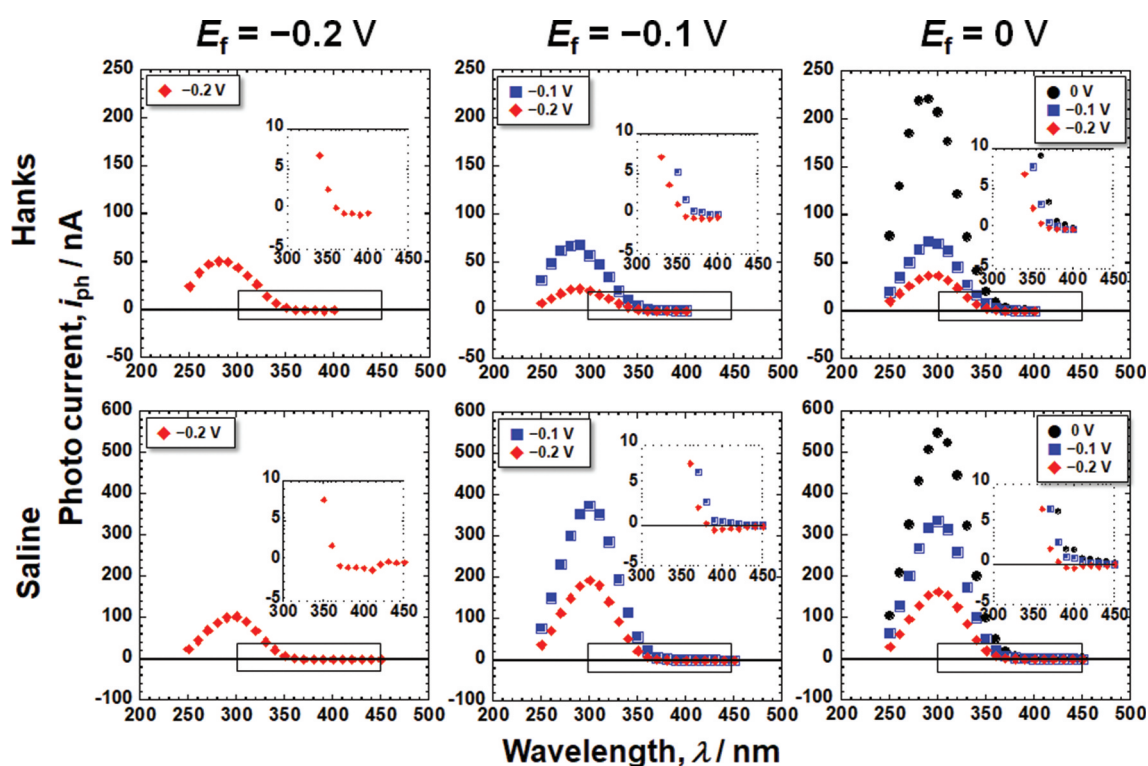


**Figure 3.** Photocurrent responses of the passive films formed on Ti in Hanks and saline.



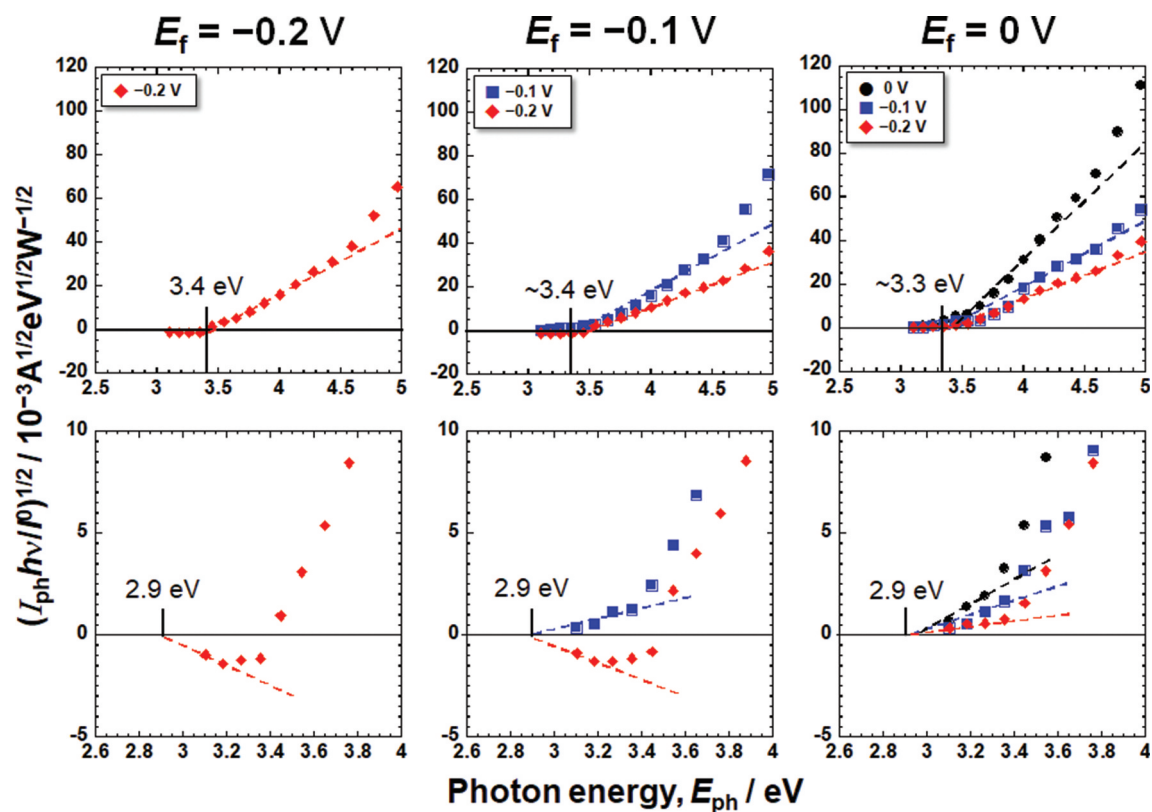


Figure 4. Photoelectrochemical action spectra calculated from the steady photocurrent in Hanks shown in Figure 3.

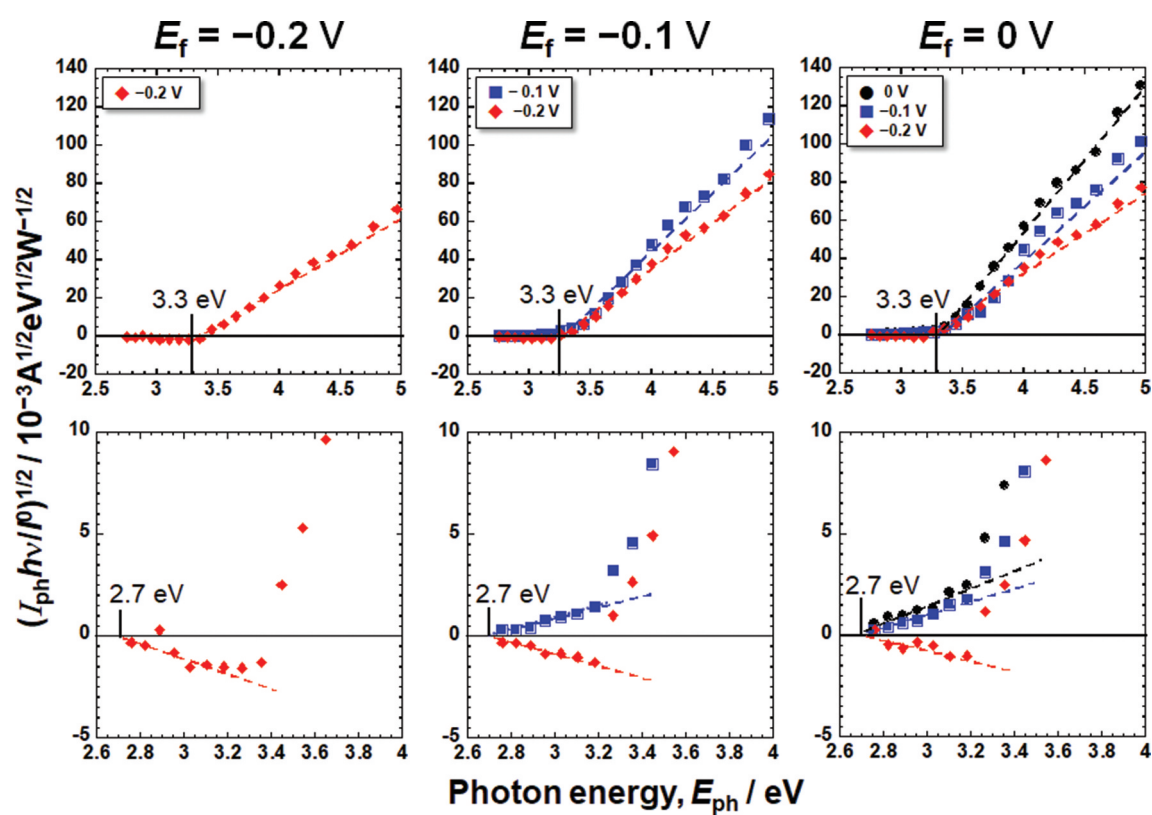


Figure 5. Photoelectrochemical action spectra calculated from the steady photocurrent in saline shown in Figure 3.

### 3.3 X-ray photoelectron spectroscopy

Titanium and oxygen were detected in all the Ti specimens. Carbon and nitrogen were also detected in the contaminated layer. In addition to the above elements, calcium and phosphorus were detected in specimens polarized in Hanks. No peak originating from  $\text{CO}_3^{2-}$  was observed at approximately 289.6 eV [24]. The Ti 2p, O 1s, Ca 2p, and P 2p electron energy region spectra obtained from Ti polarized at an  $E_f$  of 0 V are shown in Figure 6. Figure 6 shows the deconvolution of the spectrum in the Ti 2p electron energy region. The Ti 2p spectrum contains four doublets corresponding to the metallic state of  $\text{Ti}^0$  and the oxide states of  $\text{Ti}^{2+}$ ,  $\text{Ti}^{3+}$ , and  $\text{Ti}^{4+}$ . The binding energy of each valence state of titanium was determined from the previously published data [5]. The binding energy of the peak originating from  $\text{Ti}^{4+}$  before polarization was 458.8 eV and after polarization, it was 458.8–459.0 eV in both Hanks and saline. In addition, the  $[\text{Ti}^{4+}]/([\text{Ti}^{2+}] + [\text{Ti}^{3+}] + [\text{Ti}^{4+}])$  ratio, calculated from the integrated intensities of the component peaks, was almost constant at 0.78–0.82 before and after polarization in Hanks and saline. In Figure 6, the O 1s region spectrum contains three component peaks originating from oxide,  $\text{O}^{2-}$ ; hydroxyl groups or hydroxide,  $\text{OH}^-$ ; and adsorbed water or hydrate,  $\text{H}_2\text{O}$  [25]. The  $\text{OH}^-$  peak included a peak from the phosphate oxygen, but the proportion of the latter was small. The  $[\text{OH}^-]/[\text{O}^{2-}]$  ratios are shown in Figure 7. The ratios increased after polarization and those were the same at  $-0.2$  V both in Hanks and saline. The ratio in Hanks

significantly decreased with the increase in  $E_f$ , while that in saline was almost constant independent of  $E_f$ . Therefore, the ratio in saline was significantly larger than that in Hanks at 0 V. The binding energy of the Ca 2p<sub>3/2</sub> electron was 347.6–347.7 eV (Figure 6), indicating that calcium existed as  $\text{Ca}^{2+}$  [26, 27]. The binding energy of the P 2p region peak was 133.9–134.2 eV, indicating that phosphorus existed as phosphate (Figure 6) [22,28]. Therefore, it can be concluded that the calcium and phosphorus ions exist in the passive film as calcium and phosphate ions and sometimes form calcium phosphate on the passive film.

The relative concentrations of Ti, O, Ca, and P in the passive film without the Ti substrate were calculated by assuming that the total amount of these elements was 100 at.%, as presented in Table 1. It is evident that after polarization in Hanks, calcium and phosphate ions were incorporated into the passive film, but their amounts did not significantly change with increasing  $E_f$ . This table also contains ratios of calcium concentration to phosphorus concentration,  $[\text{Ca}]/[\text{P}]$ . The  $[\text{Ca}]/[\text{P}]$  ratios slightly increased with  $E_f$ , while no significant difference was observed. The thickness of the passive film increased slightly after polarization. The thickness in Hanks was comparable to or smaller than that in saline, despite the incorporation of calcium and phosphate ions or the formation of calcium phosphate.

The valence-band energy-region spectra are shown in Figure 8. The spectra were superimposed on those from the passive film and Ti substrate. In anatase, the

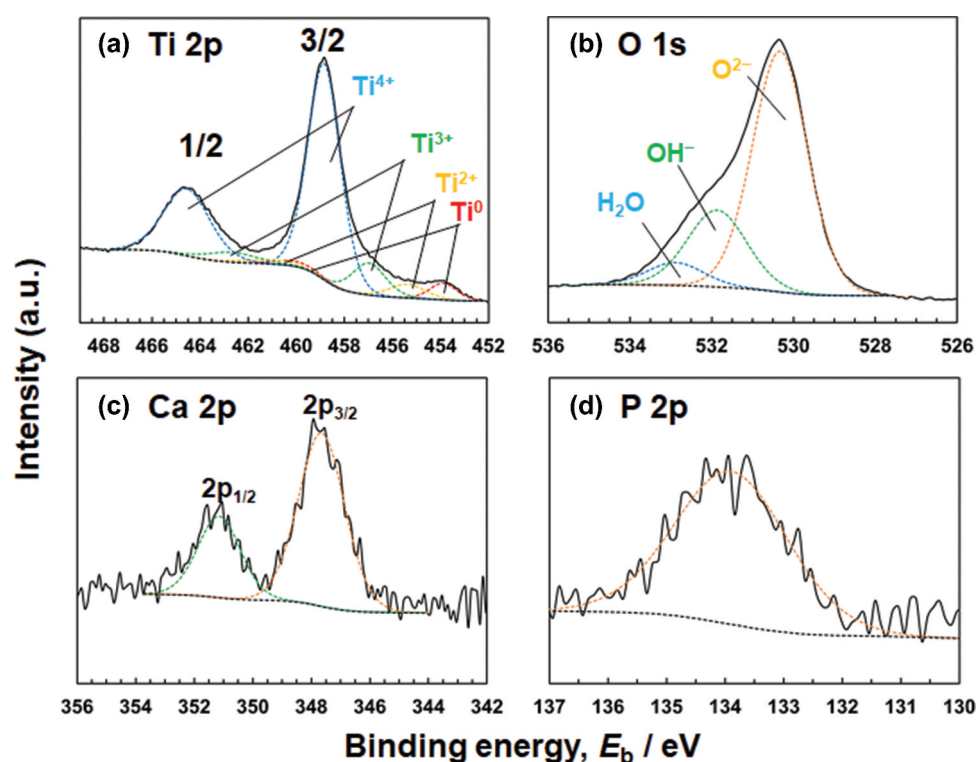


**Figure 6.** (a) Ti 2p, (b) O 1s, (c) Ca 2p, and (d) P 2p electron energy region spectra obtained from Ti after polarization at 0 V in Hanks for 1 h.

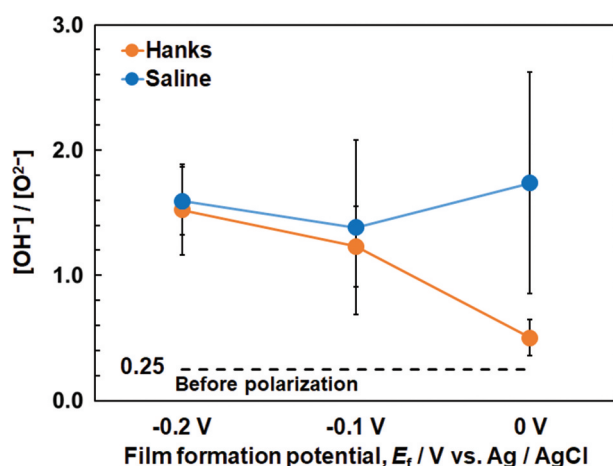


**Figure 7.**  $[\text{OH}^-]/[\text{O}^{2-}]$  ratios calculated from O 1s electron energy region spectra of Ti before and after polarization at each film formation potential,  $E_f$  ( $n = 3$ ).

valence band region contains two peaks at  $\sim 6$  and  $\sim 8$  eV, which correspond mainly to  $\pi$  (non-bonding) and  $\sigma$  (bonding) of O 2p orbitals, respectively [28]. The  $3\sigma$  orbital of  $\text{OH}^-$  appears at a binding energy of  $\sim 10.8$  eV [29]. The water molecule and  $3\sigma$  orbital of the dissociated water lie at approximately 13 and 11 eV, respectively [30]. The maximum energy of the valence band,  $E_v$ , against the Fermi energy,  $E_F$ , was determined by linearly extrapolating the fermi-level-side slope of the valence band peak on the baseline [31]. The  $E_v$  was found to be 2.8–2.9 eV in Hanks and 2.8–3.0 eV in saline, while that in the polished Ti without polarization was 2.8 eV.

#### 4. Discussion

XPS results revealed that the passive film on Ti consisted mainly of very thin  $\text{TiO}_2$  containing small amounts of  $\text{Ti}_2\text{O}_3$  and  $\text{TiO}$ , along with hydroxyl groups and water (Figure 6). These results are in accordance with those of previous studies [5–7]. In addition, the composition is probably graded; more  $\text{Ti}^{4+}$  and  $\text{OH}^-$  exist near the surface of the film [6]. The passive film on Ti is non-stoichiometric  $\text{TiO}_2$  containing  $\text{Ti}_2\text{O}_3$  and  $\text{TiO}$  that are electro conductive materials. However, the effect of  $\text{Ti}_2\text{O}_3$  and  $\text{TiO}$  on the resultant  $E_g$  is unclear in this study. On the other hand, a large number of hydroxyl groups were detected using XPS. Therefore, similar to the passive film formed on Fe-Cr

alloys, the passive film on Ti is assumed to consist of two layers [32]: inner oxide and outer hydroxide. After polarization, the  $[\text{OH}^-]/[\text{O}^{2-}]$  ratios increased in the passive films of both the Hanks and saline (Figure 7). The ratio in Hanks significantly decreased with the increase of  $E_b$ , probably caused by the formation of calcium phosphate. As a result, relative concentration of O at 0 V in Hanks were significantly smaller than those under other conditions (Table 1) because of the decrease of  $\text{OH}^-$ . The  $[\text{OH}^-]/[\text{O}^{2-}]$  ratios of the passive films on Co–28Cr–6Mo alloy (ASTM F799–95), Co–Ni–Cr–Mo alloy (ASTM F562), and 316 L-type stainless steel even before polarization were 2.9, 2.7, and 1.93 in a detection angle of  $37^\circ$ , respectively [33–35]. Therefore, the  $[\text{OH}^-]/[\text{O}^{2-}]$  ratio in the surface oxide film on Ti was much smaller than that on the Co–Cr alloys and 316 L-type stainless steel. The thickness of the passive film on Ti is much larger than that on Co–Cr alloys and 316 L-type stainless steel; thus, the relative thickness of the hydroxide layer and the relative amount of hydroxyl groups decrease.

The thickness of the passive film was increased by 0.4–1.0 nm by polarization (Table 1). As the concentrations of  $\text{Na}^+$  and  $\text{Cl}^-$  were almost the same in Hanks and saline, and other elements contained in Hanks were not contained in saline, the difference between the passive films formed in Hanks and those formed in saline may be due to the incorporation of calcium and phosphate ions or the formation of calcium phosphate in Hanks.

The  $E_g$  of the passive film formed in Hanks, 3.3–3.4 eV, was comparable or slightly larger than that in saline, 3.3 eV, independent of  $E_f$  and  $E_m$  (Figures 4 and 5). Interestingly, the  $E_g$ s of the outer layer were identical for all the  $E_f$  and  $E_m$  in each solution: 2.9 eV in Hanks and 2.7 eV in saline. Even in the lower photon energy region,  $E_g$  in Hanks was larger than that in saline. The  $E_g$  of hydroxyapatite was determined experimentally as  $>6$  eV and theoretically as 4.95 eV [36], whereas other studies reported it as 5.4 eV [37] and 4.51 eV [38]. The  $E_g$  of  $\alpha$ -tricalcium phosphate (TCP) is 4.89 eV, and that of  $\beta$ -TCP is 5.25 eV [38]. These values are much larger than those of  $\text{TiO}_2$ . The formation of calcium phosphate in Hanks probably increases  $E_g$  of the inner and outer layers.

The  $E_g$  values of the passive film and the slope  $C$  of the photoelectrochemical action spectrum were obtained, as shown in Figures 4 and 5. As mentioned

**Table 1.** Relative concentrations of elements,  $[\text{Ca}]/[\text{P}]$  ratios, and thickness of the passive film formed on Ti ( $n = 3$ ).

Electrolyte	Film formation potential, $E_f$ /V	Relative concentration (at.%)				$[\text{Ca}]/[\text{P}]$	Thickness, d/nm
		Ti	O	Ca	P		
Before polarization		28.8 $\pm$ 1.2	71.2 $\pm$ 1.0	–	–	–	5.9 $\pm$ 0.2
Hanks	–0.2	13.2 $\pm$ 1.6	85.4 $\pm$ 2.1	0.5 $\pm$ 0.3	1.0 $\pm$ 0.4	0.5 $\pm$ 0.2	6.5 $\pm$ 0.2
	–0.1	14.4 $\pm$ 2.2	84.1 $\pm$ 2.2	0.6 $\pm$ 0.2	1.0 $\pm$ 0.1	0.6 $\pm$ 0.3	6.4 $\pm$ 0.4
	0	22.8 $\pm$ 1.5	76.1 $\pm$ 1.9	0.5 $\pm$ 0.1	0.7 $\pm$ 0.2	0.7 $\pm$ 0.2	6.3 $\pm$ 0.1
Saline	–0.2	14.1 $\pm$ 2.4	85.9 $\pm$ 2.4	–	–	–	6.4 $\pm$ 0.4
	0.1	11.0 $\pm$ 2.5	89.0 $\pm$ 2.5	–	–	–	6.9 $\pm$ 0.4
	0	13.5 $\pm$ 6.5	86.5 $\pm$ 6.5	–	–	–	6.9 $\pm$ 0.6



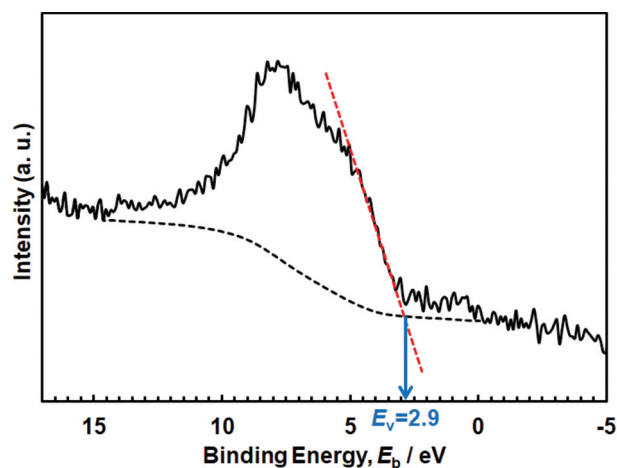


**Figure 8.** Valence band region spectra of Ti after polarization at 0 V in Hanks for 1 h and the determination of the maximum energy of valence band,  $E_v$ .

above,  $E_g$  of the outer layer is much smaller than that inside the passive film. The passive film on Ti behaved as an  $n$ -type semiconductor. However, the photocurrents at the lower photon energy region at the  $E_f$  of  $-0.2$  V and  $-0.1$  V showed negative values at low  $E_m$  (Figures 4 and 5). We assume that the outer layer, where the band gap is small, is an  $n$ -type semiconductor and that the outer layer generates space charge layers at both the film–electrolyte interface and the outer layer–inner layer interface. The photocurrent changed from positive to negative with decreasing measurement potential,  $E_m$ , because the gradients of the two space-charge layers were opposite. This phenomenon has been observed in a passive film on an Fe–Cr alloy with a  $p$ -type inner layer and an  $n$ -type outer layer [18]. The same phenomenon was observed in this study, even though both the inner and outer layers were  $n$ -type. Further discussion is necessary for the comprehension of this observation.

The  $E_g$  of the passive film on Ti anodized in  $H_2SO_4$  is  $3.25 \pm 0.05$  eV [12], whereas that anodized in artificial seawater is 3.4–3.7 eV and that anodized in borate buffer solution is 3.1 eV. After thermal oxidation at  $400^\circ\text{C}$  for 1 h, the  $E_g$  of the passive film on Ti is 3.4–

3.7 eV [14]. Meanwhile, the  $E_g$  values of the passive films formed in Hanks and saline in this study, 3.2–3.4 eV, were almost the same as those in previous studies. The  $E_g$  of  $TiO_2$  ceramics, rutile and anatase, are 3.0 eV and 3.2 eV, respectively. Therefore,  $E_g$  of the passive film formed during anodic oxidation is comparable to or larger than that of  $TiO_2$  ceramics, while in the outermost surface of the passive film, it is smaller than that of  $TiO_2$  ceramics.

From the above results and discussion, the electronic band structures of the passive film formed on Ti in Hanks and saline are shown in Figure 9. The  $E_g$  of the inner layer in Hanks was not constant but changed with depth because slope C was not constant but gradually decreased with decreasing photon energy (Figure 4). The band structure of the outer hydroxide layer was based on our previous study [16–18]. In the case of Hanks,  $E_g$  in the inner oxide layer was 3.3–3.4 eV. In the outermost surface layer,  $E_g$  was much lower (2.9 eV). In saline,  $E_g$  was 3.3 eV in the inner oxide layer and 2.7 eV in the outermost layer. In the inner oxide layer of Hanks,  $E_g$  was the same as or larger than that of saline, while  $E_v$ , the energy difference between  $E_F$ , the Fermi energy of the Ti substrate, and that of the valence band of the inner oxide layer, was 2.8–2.9 eV in Hanks and 2.8–3.0 eV in saline. Therefore, the minimum energy of the conduction band,  $E_c$ , against  $E_F$  in Hanks was larger than that in saline.

Zr forms a highly stable and protective passive film, and the reactivity of Zr is much smaller than that of Ti [39]. In the case of the passive film on Zr,  $E_g$  is 3.01–3.47 eV in the outer hydroxide layer and 4.44–4.91 eV in the inner oxide layer [40]. The passive film on Zr consists mainly of  $ZrO_2$  with hydroxyl groups. The  $E_g$  is 4.27–4.93 eV by theory and 5.78–6.1 eV by experiment that varies according to the crystal systems [41]. These values are much larger than those for  $TiO_2$  and the passive film on Ti. Therefore, the reactivity of a material can be determined based on  $E_g$ . The  $E_g$  values in the outermost layer are much smaller than those of  $TiO_2$  crystalline ceramics, rutile, and anatase, whereas the values in the inner layer are slightly larger than or almost the same as those of  $TiO_2$  ceramics.

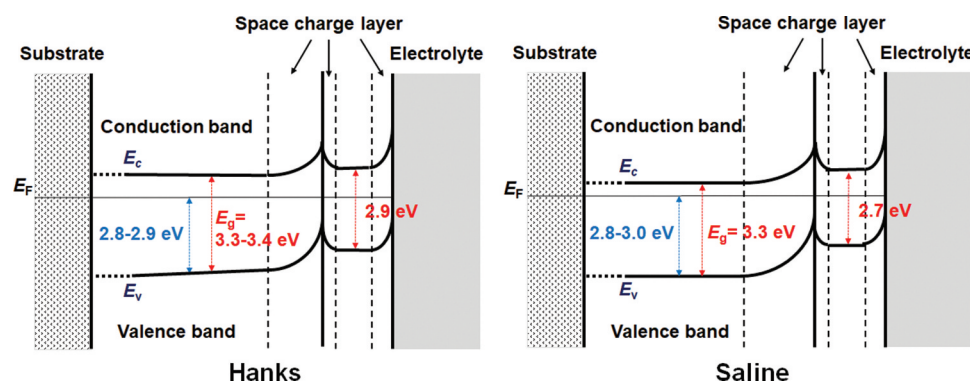


**Figure 9.** Electronic band structures of passive films formed on Ti in Hanks and saline.

A very thin and non-stoichiometric composition probably reduces the  $E_g$ . Therefore, differences in the composition, structure, and chemical state influence  $E_g$ , and thinness and non-stoichiometric composition decrease  $E_g$ . The decrease in the  $E_g$  of a material activates its reactivity, as is known for  $\text{TiO}_2$  photocatalysts. The excellent biocompatibility of Ti among the metals may be induced by the low  $E_g$  of the outermost surface layer in the passive film, which has a high corrosion resistance. Calcium phosphate is regularly formed on Ti, but not on  $\text{TiO}_2$ . Calcium phosphate formation kinetics on Ti are distinct from those on  $\text{TiO}_2$  crystalline ceramics [10]. The  $E_g$  values of the outermost surface of the passive film formed on Ti are smaller than those of the  $\text{TiO}_2$  ceramics, rutile ( $E_g = 3.0$  eV), and anatase ( $E_g = 3.2$  eV). Therefore, the Ti surface is more reactive with the surrounding environment than the  $\text{TiO}_2$  ceramic surface. This reactivity is probably one factor contributing to the excellent biocompatibility of Ti, in addition to its excellent corrosion resistance.

## 5. Conclusions

Passive films mainly consisted of a very thin  $\text{TiO}_2$  layer containing small amounts of  $\text{Ti}_2\text{O}_3$  and  $\text{TiO}$ , hydroxyl groups, and water. During polarization in Hanks, calcium and phosphate ions were incorporated or formed calcium phosphate but not in saline. Calcium phosphate and hydroxyl groups influenced the band structure.  $E_g$  was graded in Hanks but constant in saline, independent of  $E_f$  and  $E_m$ . The passive film on Ti behaved as an  $n$ -type semiconductor containing two layers: an inner oxide layer with a large  $E_g$  and an outer hydroxide layer with a small  $E_g$ . In Hanks, the value of  $E_g$  in the inner layer was 3.3–3.4 eV, whereas it was much lower in the outermost surface layer (2.9 eV). In saline,  $E_g$  was 3.3 eV in the inner layer and 2.7 eV in the outermost layer. The  $E_g$  values of the outermost surfaces of the passive films formed on Ti were smaller than those of  $\text{TiO}_2$  ceramics. Therefore, the Ti surface is more reactive with the surrounding environment than the  $\text{TiO}_2$  ceramic surface. This is probably one of the reasons for the excellent biocompatibility of Ti among metals, in addition to its excellent corrosion resistance.

## Disclosure statement

No potential conflict of interest was reported by the author(s).

## Funding

This work was financially supported by the Design & Engineering by the Joint Inverse Innovation for Materials Architecture (DEJI<sup>2</sup>MA) Project and the Viable Materials Project, Ministry of Education, Culture, Sports, Science, and Technology (MEXT), Japan.

## ORCID

Seong-Cheol Kim  <http://orcid.org/0000-0001-9344-2577>  
Takao Hanawa  <http://orcid.org/0000-0003-1688-1749>  
Tomoyo Manaka  <http://orcid.org/0000-0001-9649-2035>  
Hiroaki Tsuchiya  <http://orcid.org/0000-0001-5619-0139>  
Shinji Fujimoto  <http://orcid.org/0000-0002-7787-4190>

## References

- [1] Brunette DM, Tenvall P, Textor M, et al. Titanium in medicine. Berlin: Springer; 2001. doi:10.1007/978-3-642-56486-4
- [2] Sanderson PL, Ryan W, Turner PG. Complications of metalwork removal. *Injury*. 1992;23(1):29–30. doi:10.1016/0020-1383(92)90121-8
- [3] Hanawa T. Titanium-tissue interface reaction and its control with surface treatment. *Front Bioeng Biotechnol*. 2019;7:170. doi:10.3389/fbioe.2019.00170
- [4] Kelly EJ. Electrochemical behavior of titanium. *Mod Aspect Electrochem*. 1982;14:319–424. doi:10.3389/fbioe.2019.00170
- [5] Asami K, Chen SC, Habazaki H, et al. The surface characterization of titanium and titanium–nickel alloys in sulfuric acid. *Corros Sci*. 1993;35(1–4):43–49. doi:10.1016/0010-938X(93)90131-Y
- [6] Hanawa T, Asami K, Asaoka K. Repassivation of titanium and surface oxide film regenerated in simulated bioliquid. *J Biomed Mater Res*. 1998;40:530–538. doi:10.1002/(sici)1097-4636(19980615)40:4<530::aid-jbm3>3.0.co;2-g
- [7] Hiji A, Hanawa T, Shimabukuro M, et al. Initial formation kinetics of calcium phosphate on titanium in Hanks' solution characterized using XPS. *Surf Interface Anal*. 2021;53(2):185–193. doi:10.1002/sia.6900
- [8] Olver JW, Ross JW. On the standard potential of the titanium(iii)–titanium(ii) couple. *J Am Chem Soc*. 1963;85(17):2565–2566. doi:10.1021/ja00900a006
- [9] Wang L, Yu H, Wang K, et al. Local fine structural insight into mechanism of electrochemical passivation of titanium. *ACS Appl Mater Interfaces*. 2016;8(28):18608–18619. doi:10.1021/acsami.6b05080
- [10] Hiji A, Hanawa T, Yokoi T, et al. Time transient of calcium and phosphate ion adsorption by rutile crystal facets in Hanks' solution characterized by XPS. *Langmuir*. 2021;37:3597–3604. doi:10.1021/acs.langmuir.0c03540
- [11] Diebold U. The surface science of titanium dioxide. *Surf Sci Rep*. 2003;48:53–229. doi:10.1016/S0167-5729(02)00100-0
- [12] Di Quarto F, Piazza S, Sunseri C. The photoelectrochemistry of thin passive layers. Investigation of anodic oxide films on titanium metals. *Electrochim Acta*. 1993;38(1):29–35. doi:10.1016/0013-4686(93)80006-L
- [13] Marsh J, Gorse D. A photoelectrochemical and ac impedance study of anodic titanium oxide films. *Electrochim Acta*. 1998;43(7):659–670. doi:10.1016/S0013-4686(97)00210-7
- [14] Kim DY, Kwon HS. A study on electronic properties of passive film formed on Ti. *Corros Sci Technol*. 2003;2:212–218.
- [15] Tsuchiya H, Fujimoto S. Semiconductor properties of passive films formed on sputter-deposited Fe–18Cr alloy thin films with various additive elements. *Sci Technol Adv Mater*. 2004;5(1–2):195–200. doi:10.1016/j.stam.2003.10.014

- [16] Tsuchiya H, Fujimoto S, Shibata T. Semiconductive properties of passive films formed on Fe-18Cr in borate buffer solution. *J Electrochem Soc.* **2004**;151(2):B39–B44. doi:10.1149/1.1639163
- [17] Tsuchiya H, Fujimoto S, Shibata T. Semiconductive behavior of passive films formed on Fe-Cr alloy. *J Electroceram.* **2006**;6:9–54. doi:10.1007/s10832-006-5703-z
- [18] Fujimoto S, Tsuchiya H. Semiconductor properties and protective role of passive films of iron base alloys. *Corros Sci.* **2007**;49(1):195–202. doi:10.1016/j.corsci.2006.05.020
- [19] Shirley DA. High-resolution X-ray photoemission spectrum of the valence bands of gold. *Phys Rev B.* **1972**;5(12):4709–4714. doi:10.1103/PhysRevB.5.4709
- [20] Asami K, Hashimoto K, Shimodaira S. XPS determination of compositions of alloy surfaces and surface oxides on mechanically polished iron–chromium alloys. *Corros Sci.* **1977**;17(9):713–723. doi:10.1016/0010-938X(77)90067-1
- [21] Asami K, Hashimoto K. An XPS study of the surfaces on Fe-Cr, Fe-Co and Fe-Ni alloys after mechanical polishing. *Corros Sci.* **1984**;24(2):83–97. doi:10.1016/0010-938X(84)90039-8
- [22] Hanawa T, Ota M. Calcium phosphate naturally formed on titanium in electrolyte solution. *Biomaterials.* **1991**;12:767–774. doi:10.1016/0142-9612(91)90028-9
- [23] Tanaka Y, Nakai M, Akahori T, et al. Characterization of air-formed surface oxide film on Ti–29Nb–13Ta–4.6Zr alloy surface using XPS and AES. *Corros Sci.* **2008**;50(8):2111–2116. doi:10.1016/j.corsci.2008.06.002
- [24] Hammond JS, Holubka JW, DeVries JE, et al. The application of X-ray photo-electron spectroscopy to a study of interfacial composition in corrosion-induced paint de-adhesion. *Corros Sci.* **1981**;21(3):239–253. doi:10.1016/0010-938X(81)90033-0
- [25] Asami K, Hashimoto K. The X-ray photo-electron spectra of several oxides of iron and chromium. *Corros Sci.* **1977**;17(7):559–570. doi:10.1016/S0010-938X(77)80002-4
- [26] Wagner CD. Photoelectron and Auger energies and the Auger parameter: a data set. In: Briggs D Seah MP, editors. *Practical surface analysis*. 2nd ed. New York: Wiley; **1990**. pp. 595–634. doi:10.1002/jctb.280530219
- [27] Hanawa T, Ota M. Characterization of surface film formed on titanium in electrolyte using XPS. *Appl Surf Sci.* **1992**;55(4):269–276. doi:10.1016/0169-4332(92)90178-Z
- [28] Orendorcz A, Wüsten J, and Ziegler C, et al. Photoelectron spectroscopy of nanocrystalline anatase TiO<sub>2</sub> films. *Appl Surf Sci.* **2005**;252(1):85–88. doi:10.1016/j.apsusc.2005.02.002
- [29] Fusi M, Maccallini E, Caruso T, et al. Surface electronic and structural properties of nanostructured titanium oxide grown by pulsed laser deposition. *Surf Sci.* **2011**;605(3–4):333–340. doi:10.1016/j.susc.2010.10.039
- [30] Kurtz RL, Stock-Bauer R, Msdey TE, et al. Synchrotron radiation studies of H<sub>2</sub>O adsorption on TiO<sub>2</sub>(110). *Surf Sci.* **1989**;218(1):178–200. doi:10.1016/0039-6028(89)90626-2
- [31] Singh AP, Kodan N, Mehta BR. Enhancing the photo-electrochemical properties of titanium dioxide by thermal treatment in oxygen deficient environment. *Appl Surf Sci.* **2016**;372:63–69. doi:10.1016/j.apsusc.2016.03.072
- [32] Lynch B, Wiame F, Maurice V, et al. XPS study of oxide nucleation and growth mechanisms on a model FeCrNiMo stainless steel surface. *Appl Surf Sci.* **2022**;575:151681. doi:10.1016/j.apsusc.2021.151681
- [33] Hanawa T, Hiromoto S, Asami K. Characterization of the surface oxide film of a Co–Cr–Mo alloy after being located in quasi-biological environments using XPS. *Appl Surf Sci.* **2001**;183(1–2):68–75. doi:10.1016/S0169-4332(01)00551-7
- [34] Nagai A, Tsutsumi Y, Suzuki Y, et al. Characterization of air-formed surface oxide film on a Co–Ni–Cr–Mo alloy (MP35N) and its change in Hanks' solution. *Appl Surf Sci.* **2012**;258(14):5490–5498. doi:10.1016/j.apsusc.2012.02.057
- [35] Hanawa T, Hiromoto S, Yamamoto A, et al. XPS characterization of the surface oxide film of 316L stainless steel samples that were located in quasi-biological environments. *Mater Trans.* **2002**;43(12):3088–3092. doi:10.2320/matertrans.43.3088
- [36] Tsukada M, Wakamura M, Yoshida N, et al. Band gap and photocatalytic properties of Ti-substituted hydroxyapatite: comparison with anatase-TiO<sub>2</sub>. *J Mol Catal a.* **2011**;338:18–23. doi:10.1016/j.molcata.2011.01.017
- [37] Calderín L, Stott MJ, Rubio A. Electronic and crystallographic structure of apatites. *Phys Rev B.* **2003**;67(13):134106. doi:10.1103/PhysRevB.67.134106
- [38] Liang L, Rulis P, Ching WY. Mechanical properties, electronic structure and bonding of  $\alpha$ - and  $\beta$ -tricalcium phosphates with surface characterization. *Acta Biomater.* **2010**;6(9):3763–3771. doi:10.1016/j.actbio.2010.03.033
- [39] Tsutsumi Y, Nishimura D, Doi H, et al. Difference in surface reactions between titanium and zirconium in Hanks' solution to elucidate mechanism of calcium phosphate formation on titanium using XPS and cathodic polarization. *Mater Sci Eng C.* **2009**;29(5):1702–1708. doi:10.1016/j.msec.2009.01.016
- [40] Kim BY, Park CJ, Kwon H. Effect of niobium on the electronic properties of passive films on zirconium alloys. *J Electroanal Chem.* **2005**;576(2):269–276. doi:10.1016/j.jelechem.2004.11.002
- [41] French RH, Glass SJ, Ohuchi FS, et al. Experimental and theoretical determination of the electronic structure and optical properties of three phases of ZrO<sub>2</sub>. *Phys Rev B.* **1994**;49(8):5133–5142. doi:10.1103/PhysRevB.49.5133